JACS
JOURNAL OF THE AMERICAN CHEMICAL SOCIETY
pubs.acs.org/JACS
Article

Electron–Nuclear Dynamics Accompanying Proton-Coupled Electron Transfer

Yusuke Yoneda,[▽] S. Jimena Mora,[▽] James Shee,[▽] Brian L. Wadsworth,[▽] Eric A. Arsenault, Diptarka Hait, Gerdenis Kodis, Devens Gust, Gary F. Moore, Ana L. Moore, Martin Head-Gordon, Thomas A. Moore, and Graham R. Fleming*

Cite This: *J. Am. Chem. Soc.* 2021, 143, 3104–3112

Read Online

ACCESS | Metrics & More | Article Recommendations | Supporting Information

ABSTRACT: Although photoinduced proton-coupled electron transfer (PCET) plays an essential role in photosynthesis, a full understanding of the mechanism is still lacking due to the complex nonequilibrium dynamics arising from the strongly coupled electronic and nuclear degrees of freedom. Here we report the photoinduced PCET dynamics of a biomimetic model system investigated by means of transient IR and two-dimensional electronic–vibrational (2DEV) spectroscopies, IR spectroelectrochemistry (IRSEC), and calculations utilizing long-range-corrected hybrid density functionals. This collective experimental and theoretical effort provides a nuanced picture of the complicated dynamics and synergistic motions involved in photoinduced PCET. In particular, the evolution of the 2DEV line shape, which is highly sensitive to the mixing of vibronic states, is interpreted by accurate computational modeling of the charge separated state and is shown to represent a gradual change in electron density distribution associated with a dihedral twist that occurs on a 120 fs time scale.

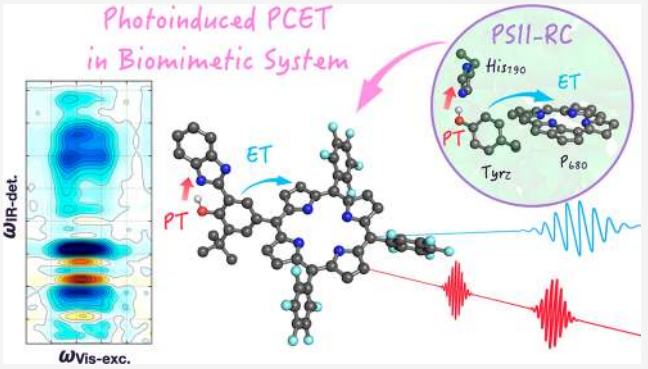

INTRODUCTION

Proton-coupled electron transfer (PCET) is ubiquitous in chemistry and biology.[1−8] In the energy transducing membranes of all cells, PCET serves to reversibly couple energy linked redox processes to the generation and use of proton-motive force. PCET is crucial to the favorable energetics of water splitting by the photosystem II reaction center (PSII-RC) of green plants, cyanobacteria, and algae where it is one of the iconic processes in biology. Following excitation and charge separation (CS) in the PSII-RC, the highly oxidizing chlorophyll (P_{680}^{+}) oxidizes the water-oxidizing CaO_5Mn_4 catalytic cluster via an electron transfer relay comprised of a tyrosine (Tyr_Z) histidine (His190) pair.[9,10] This relay functions by using PCET associated with the reversible transfer of the phenolic proton of Tyr_z to the imidazole of His190 during the redox cycle to control both the thermodynamics and kinetics of water oxidation by P_{680}^{+}.[2,7] Inspired by natural biological systems, many artificial photosynthetic systems have been developed to achieve highly efficient light energy conversion and to understand the underlying mechanism of PCET.[8,11−18] Our model for P_{680} and the H-bonded Tyr_z–His190 pair is benzimidazole-phenol-pentafluorophenylporphyrin ($BIPPF_{15}$)[8,11−15,17] (Figure 1a), where the porphyrin mimics P_{680} and benzimidazole-phenol mimics His190 and Tyr_z, respectively.

PCET reactions can be described as nonadiabatic transitions between diabatic charge-localized vibronic states because the motions of electrons, protons, and surrounding media are often strongly coupled.[3,5] The high degrees of dimensionality and mixing especially complicate photoinduced PCET dynamics, thus making the study of such phenomena challenging. Despite these complexities, recent work has begun to advance our understanding of photoinduced PCET reactions. For example, the relation between free energy gaps and electron transfer (ET) kinetics was successfully described by nonadiabatic PCET theory.[16] Another study revealed that optical excitation can directly prepare the electron–proton transfer photoproduct.[19] However, it is important to note that all of these previous time-resolved spectroscopic studies have regarded the photoinduced PCET reaction as a state-to-state transition.[16,19−21] However, contrary to this treatment, electronically excited states are typically best described via mixing of different electronic configurations, and the degree of

Received: October 6, 2020
Published: February 18, 2021

https://dx.doi.org/10.1021/jacs.0c10626
J. Am. Chem. Soc. 2021, 143, 3104–3112

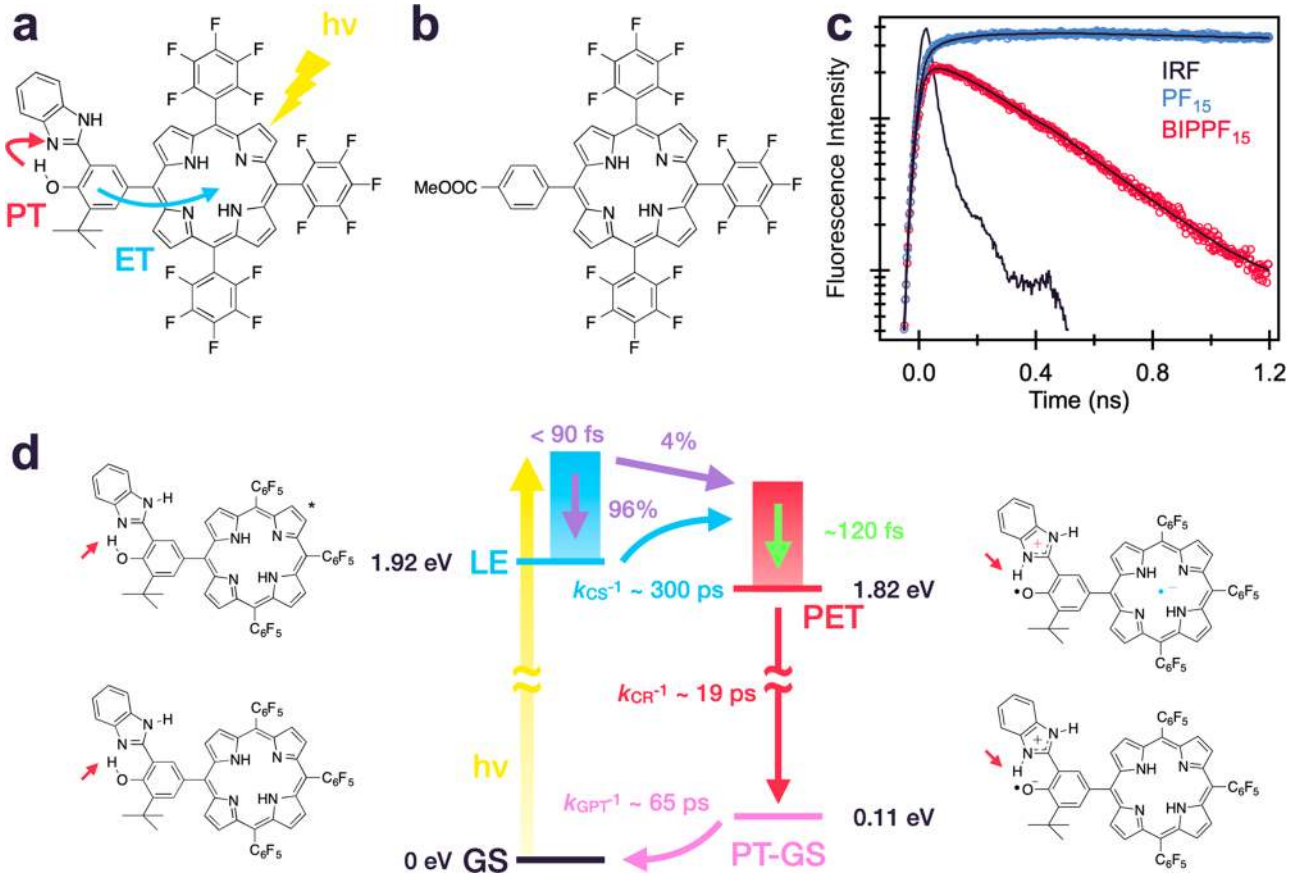

Figure 1. Biomimetic photoinduced PCET system. (a) Molecular structure of the biomimetic photoinduced PCET system ($BIPPF_{15}$) and (b) reference system (PF_{15}). (c) Time-resolved fluorescence of PF_{15} and $BIPPF_{15}$ in acetonitrile with excitation at 583 nm and emission detection at 710 nm. Open circles: raw data. Solid lines: fit with 9.8 ns and 272 ps (292 ps in deuterated acetonitrile) lifetimes for PF_{15} and $BIPPF_{15}$, respectively. Both compounds had the same optical density at the excitation wavelength, and the kinetics was collected for the same amount of time. The data at longer time is provided in Figure S13. (d) Schematic of photoinduced PCET dynamics in deuterated acetonitrile. On photoexcitation, the initial Franck–Condon population branches into two pathways (purple arrows) toward: (i) a relaxed locally excited (LE) state which is followed by a slow, activated PCET pathway (blue arrow) with $k_{CS}^{-1} \sim 300$ ps (calculated from fluorescence decay lifetimes in deuterated acetonitrile) to the unrelaxed proton and electron transferred (PET) state (vide infra) and (ii) an unrelaxed PET state within 90 fs. From there, the unrelaxed PET state rapidly evolves toward the relaxed product with concomitant charge transfer on a time scale of 120 fs (green arrow). The PET state relaxes to a proton transferred-ground state (PT-GS) with $k_{CR}^{-1} \sim 19$ ps through charge recombination (CR) (red arrow) and subsequently returns to the original GS with $k_{GPT}^{-1} \sim 65$ ps (pink arrow). The energy levels of LE (1.92 eV), PET (1.82 eV), and PT-GS (0.11 eV) states were estimated by absorption and fluorescence spectra, the Rehm–Weller equation, and quantum chemical calculation, respectively.

mixing can change throughout the course of the movement of electrons and protons.[22,23] Moreover, photoexcitation leads a system into a nonequilibrium distribution of many vibronic energy levels.[24] For the above reasons, the mechanism of ultrafast photoinduced PCET remains essentially unexplored. If the process has a free energy barrier, dynamical studies of the system are incapable of following the evolution of the electronic/vibrational distribution, as the fractional population of states other than the initial and final states is very small at all times. In contrast, ultrafast relaxation proceeding without a barrier has the potential to enable tracking of the continuous evolution of the electronic and vibrational distribution. Such measurements, then, can provide a significantly more nuanced view of PCET. As we show below, the molecule $BIPPF_{15}$ (Figure 1a) undergoes excited state PCET on two time scales—ultrafast (<90 fs) (4%) and a few hundred ps (270–290 ps) (96%), with the latter, relaxed PCET likely having to overcome a free energy barrier. For the reasons just outlined, we focus on the ultrafast PCET, as this process reveals details that must underlie many PCET reactions on all time scales but are simply not discernible in these systems. For completeness in the Supporting Information, we give a thorough analysis of the longer time scale kinetics and spectroscopy. The recently developed spectroscopic technique, two-dimensional electronic–vibrational (2DEV) spectroscopy, which correlates electronic and nuclear evolution, is particularly suited for studies of PCET.[25−29] Unlike degenerate multidimensional Fourier transform spectroscopies, such as two-dimensional electronic or infrared spectroscopy, 2DEV has a number of advantages for elucidating the nonequilibrium dynamics of vibronic states. These include the following: (i) simultaneous spectral resolution along both the visible excitation axis and the infrared detection axis, which enables the clear assignment of transient species as the IR frequencies are now dispersed along the excitation axis; (ii) high spectral sensitivity to the mixing of electronic/vibronic states, which significantly alters vibrational transition moments; and (iii) identification of the

https://dx.doi.org/10.1021/jacs.0c10626
J. Am. Chem. Soc. 2021, 143, 3104−3112

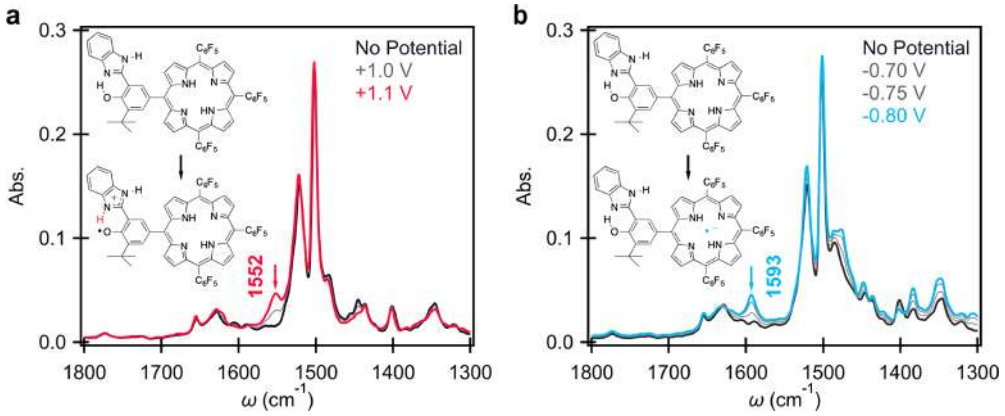

Figure 2. IRSEC spectra of $BIPPF_{15}$. (a) Upon oxidation of $BIPPF_{15}$, a band at 1552 cm^{-1} appeared and is assigned to benzimidazolium cation formation following a PT from the phenol moiety. (b) Upon reduction of $BIPPF_{15}$, a band at 1593 cm^{-1} appeared, which is indicative of porphyrin radical anion formation. Spectra were recorded in dry deuterated acetonitrile solution with 0.1 M $TBAPF_6$. The colored curves show oxidized (red) or reduced (blue) species. In parts a and b, the black curve indicates the neutral species. The applied potentials indicated in the figure legend are versus a silver wire reference electrode (see the Experimental Methods section for further details).

center line slope (CLS) of the spectral features, which is related to a cross-correlation of vibrational and electronic dipoles and is very sensitive to significant changes in electronic structure.

Previously, the excited state dynamics of a high-potential porphyrin bearing two pentafluorophenyl groups (PF_{10}), $BIPPF_{10}$, was investigated by means of transient absorption spectroscopy.[11,13] In acetonitrile, upon photoexcitation of the porphyrin moiety, the lifetime of $BIPPF_{10}$ was determined to be 430 ps—significantly shorter than that of PF_{10} (~10 ns)—suggesting that the excited state is quenched by ET. However, the spectrum of the CS state was not observed. Thus, it was concluded that the system undergoes inverted kinetics, wherein CS is slower than CR. The slower CS reaction was rationalized by the small driving force.[11,13] In the above study, the broad and featureless transient spectra of the PF_{10} ion in the visible range made it difficult to detect the PCET product during the course of the reaction and therefore even harder to potentially resolve additional fast PCET pathways. Furthermore, the relatively large molecules involved rendered the CS states challenging to accurately and tractably describe with traditional quantum chemical calculations.

In this study, we investigated the excited state dynamics of 5-[4-hydroxy-3-(benzimidazole-2-yl)-5-*tert*-butylphenyl]-10,15,20-*tris*(pentafluorophenyl)porphyrin[30] ($BIPPF_{15}$, Figure 1a) by means of transient IR and 2DEV spectroscopies and specialized density functional theory (DFT) calculations. Compared to $BIPPF_{10}$, $BIPPF_{15}$ contains an additional pentafluorophenyl group, resulting in a less negative $E_{1/2}$ value for the porphyrin/porphyrin$^-$ redox couple; thus, a larger driving force and a faster rate of photoinduced ET can be expected. By combining IR spectroelectrochemical (IRSEC) measurements with electronic−vibrational spectroscopies, we can clearly track the PT and ET dynamics associated with the BIP radical cation and porphyrin radical anion, respectively.[8,14,15] The spectroscopic data was complemented by *ab initio* electronic structure calculations using a long-range-corrected (LRC) hybrid functional,[31,32] which can be optimally and nonempirically tuned to provide a robust and efficient characterization of the CS state, even for large molecules.[33−35] As a control, we also investigated the dynamics of the reference porphyrin system, 5-(4-carbomethoxyphenyl)-10,15,20-*tris*(pentafluorophenyl)porphyrin (PF_{15}, Figure 1b).[30] Details of all of the experimental and theoretical methods used in this work are collected together in the Supporting Information.

RESULTS AND DISCUSSION

Fluorescence Lifetime Measurement. Figure 1c shows time-resolved fluorescence decays of PF_{15} and $BIPPF_{15}$ in acetonitrile. The lifetime of $BIPPF_{15}$ was 272 ps (292 ps in deuterated acetonitrile), which is much shorter than that of PF_{15} (9.8 ns), indicating that ET takes place within this time scale.

The fluorescence kinetics was collected for the same amount of time with the same experimental setup, and the excitation was set at 583 nm, where PF_{15} and $BIPPF_{15}$ have the same extinction coefficient, and at identical concentrations. Exponential fits with instrument response function (IRF) deconvolution give normalized pre-exponential factors of 1.00 versus 0.75 for PF_{15} and $BIPPF_{15}$, respectively. This indicates that some fraction of the fluorescence intensity of $BIPPF_{15}$ is lost at short times (within the IRF of the time-resolved fluorescence measurement), in agreement with ultrafast PCET occurring from unrelaxed levels, as will be discussed in detail below.

Electrochemistry. IRSEC measurements were performed to examine the change in the IR spectra following the oxidation or reduction of $BIPPF_{15}$. Upon oxidation of $BIPPF_{15}$ (Figure 2a), a new band at 1552 cm^{-1} appeared. This band is indicative of the benzimidazolium cation (NH in-plane bending vibration) generated following a PT from the phenol moiety, as observed in earlier studies.[8,14,15] Upon reduction of $BIPPF_{15}$ (Figure 2b), a new band that is characteristic of porphyrin radical anion formation was observed at 1593 cm^{-1}.[17] Quantum chemical calculations at the B3LYP/6-31G** level find a mode with similar frequency for the anion which involves only atoms of the porphyrin. Therefore, the bands at 1593 and 1552 cm^{-1} are used as evidence for ET and PT, respectively.

The midpoint potentials ($E_{1/2}$) for the $BIPPF_{15}^+/BIPPF_{15}$ and $BIPPF_{15}/BIPPF_{15}^-$ redox couples were estimated to be +1.05 and −0.83 V versus SCE, respectively, by cyclic voltammetry measurements (Figure S1). By assuming the

https://dx.doi.org/10.1021/jacs.0c10626
J. Am. Chem. Soc. 2021, 143, 3104−3112

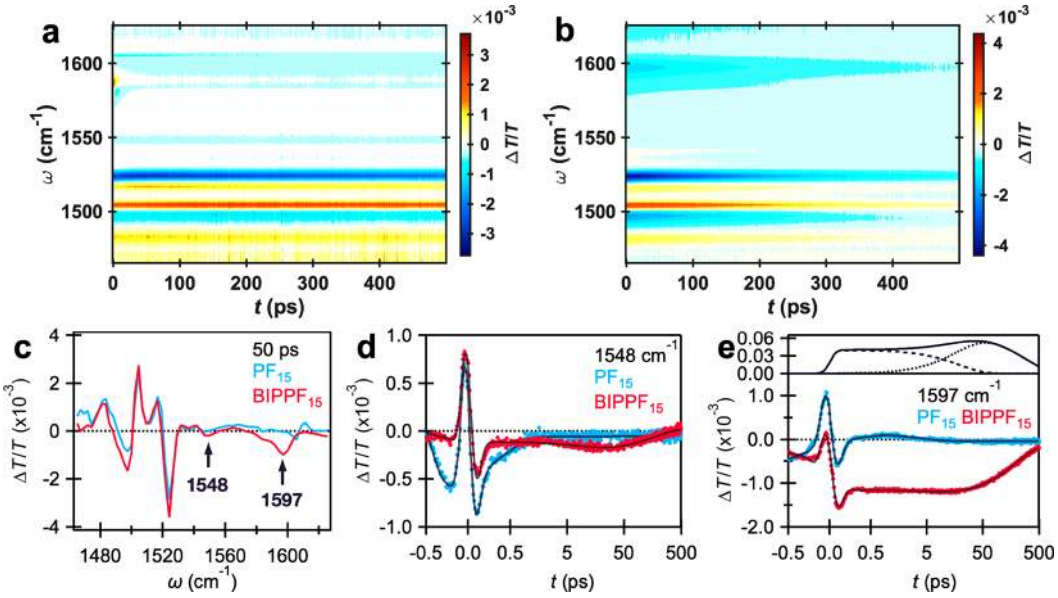

Figure 3. Transient IR dynamics of PF_{15} and $BIPPF_{15}$. Contour plot of transient IR spectra of (a) PF_{15} and (b) $BIPPF_{15}$ in dry deuterated acetonitrile. Positive signals (red contours) represent ground state bleach, and negative signals (blue contours) represent excited state absorption. (c) Transient IR spectra of PF_{15} (blue) and $BIPPF_{15}$ (red) at 50 ps. This delay time was chosen to avoid the interference from vibrational relaxation (within 10 ps) observed in PF_{15}. Time traces of the transient IR signals of PF_{15} (blue) and $BIPPF_{15}$ (red) probed at (d) 1548 cm^{-1} and (e) 1597 cm^{-1}. The time axis is linear from −0.5 to 0.5 ps and logarithmic at later delay times. The black curves show the fit results using the fitting parameters summarized in Table S2. The population dynamics of the PET state for ultrafast unrelaxed (dashed curve) and slower relaxed (dotted line curve) pathways, along with the sum total (solid curve), as obtained by the model (Figure S10) is also plotted at the top of part e. The center wavelength of excitation was 580 nm (Figure S2).

center-to-center distance between the phenol and porphyrin moieties to be l = 6.4 Å and the excited state (S_1) energy to be E_{00} = 1.92 eV, the driving force can be estimated from the Rehm−Weller equation to be ΔG = −100 meV (other parameters and details are provided in the Supporting Information). The excited state characterized by electron transfer from the phenol moiety of $BIPPF_{15}$ to the porphyrin, but without proton transfer, is designated as the CSS species in Figure 6 and is calculated to be 3.35 eV above the GS, resulting in an endergonic pathway following photoexcitation.

Transient IR Spectroscopy. Transient IR spectroscopy was applied to $BIPPF_{15}$ and PF_{15} to elucidate the excited state kinetics. For PF_{15} (Figure 3a), the reference system, photoinduced increases in transmission were observed at 1481, 1503, and 1515 cm^{-1} and are assigned to ground state bleach (GSB) signals. Excited state absorption (ESA) bands were observed at 1495, 1522, 1546, and 1606 cm^{-1}. The lifetime of PF_{15} was longer than the detection limit of our experimental setup of ∼500 ps.

The spectral features of $BIPPF_{15}$ (Figure 3b) were similar to those of PF_{15} at frequencies below 1540 cm^{-1}. However, the lifetime of $BIPPF_{15}$ (290 ps) was significantly shorter than that of PF_{15}, indicating that the excited state is quenched by ET. By comparing the spectra at frequencies above 1540 cm^{-1} (Figure 3c), three additional negative bands were observed at 1548, 1580, and 1597 cm^{-1} for $BIPPF_{15}$. The bands at 1548 and 1597 cm^{-1} were similar to those observed in the IRSEC measurements (Figure 2), indicating that both PT and ET, respectively, take place in $BIPPF_{15}$ following photoexcitation of the porphyrin moiety. Small frequency differences between the transient IR and IRSEC measurements are ascribed to the IR Stark effect. The band at 1580 cm^{-1} is likely due to a byproduct or a photodegraded sample as the relative intensity of this band changes in different measurements. It should be noted that $BIPPF_{15}$ shows larger ESA signals at 1495 and 1522 cm^{-1}; however, to avoid the influence of overlapping bands from the LE state's signal, we focus on the dynamics of the 1548 and 1597 cm^{-1} bands in the following. As noted above, both the 1548 and 1597 cm^{-1} modes are quite delocalized on BIP and PF_{15} moieties and act as reporters of the proton and electron moving, respectively, rather than as key components of the reaction coordinate.

The time traces at 1548 and 1597 cm^{-1} were analyzed to elucidate the kinetics (Figure 3d,e). Compared on a picosecond time scale, the ESAs of $BIPPF_{15}$ showed an increase in the signal intensity with a few tens of ps, while such a change was absent in PF_{15}. Here, the dynamics suggests that the PCET reaction can be viewed simply as a kinetic phenomenon where the rise of the signal reflects the CR rate in the previously proposed inverted kinetics scheme (Figure 1c where $k_{CS} \ll k_{CR}$)[13] and the small signal change can be rationalized by the relation between the rate constants for the k_{CS}^{-1} ∼300 ps (calculated from the fluorescence lifetime of $BIPPF_{15}$ and PF_{15}) and the k_{CR}^{-1} ∼19 ps (see the "Detailed Analysis of Transient IR Spectra of BIPPF15" section in the Supporting Information for details). However, the remainder of the discussion will focus on 2DEV experiments and analysis which reveals an additional ultrafast PCET pathway.

Initial evidence for such a pathway is that, notably, the ESAs of $BIPPF_{15}$ at 1548 and 1597 cm^{-1} appeared immediately after the photoexcitation. The immediate appearance of these bands suggests that a PET state is either (i) prepared directly by photoexcitation or (ii) formed via an additional nonequilibrium pathway which proceeds within our instrument response time of ∼90 fs. However, the small negative signal at 1546 cm^{-1} also appeared instantaneously for PF_{15}, suggesting the need for further data before the 1548 cm^{-1} band is assigned to PT at short times.

https://dx.doi.org/10.1021/jacs.0c10626
J. Am. Chem. Soc. 2021, 143, 3104−3112

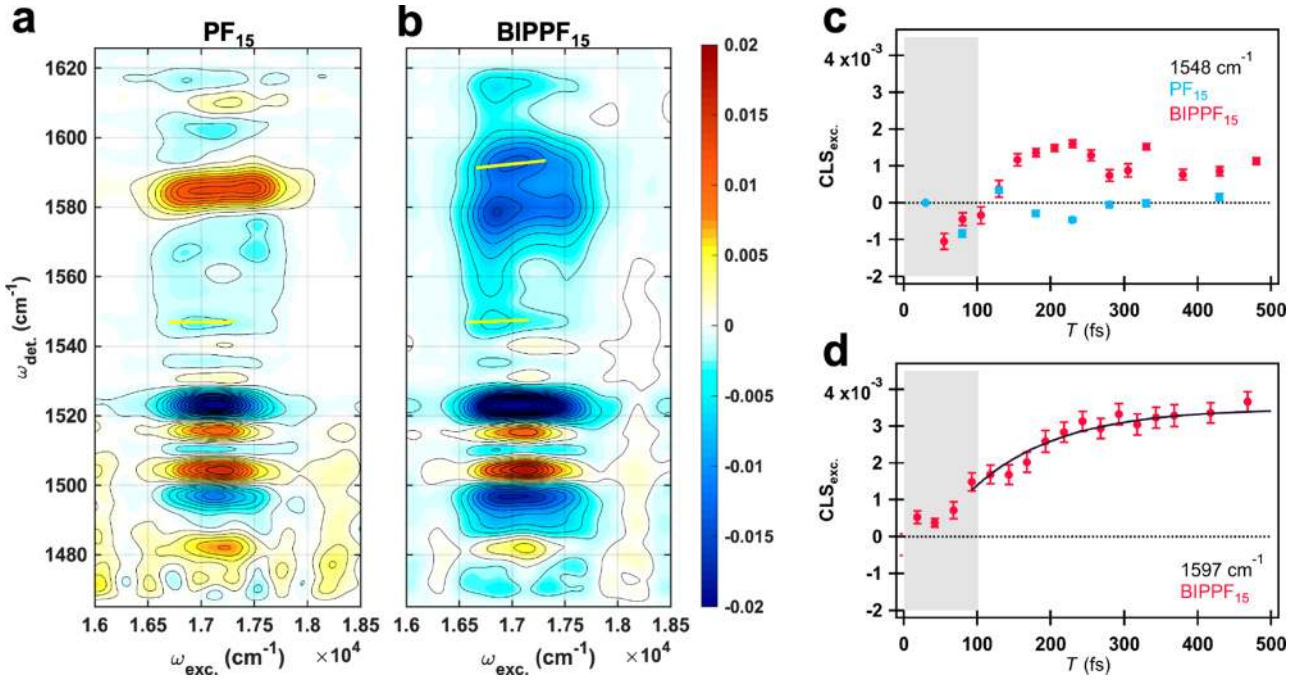

Figure 4. 2DEV spectroscopy of PF_{15} and $BIPPF_{15}$. 2DEV spectra of (a) PF_{15} and (b) $BIPPF_{15}$ at 500 fs. Positive signals (red contours) indicate ground state bleaches, and negative signals (blue contours) represent excited state absorptions. Contour levels are drawn in 5% intervals. Yellow lines indicate the CLS (with respect to the excitation axis) obtained by a linear fit of the conditional average.[27] CLS dynamics of PF_{15} (blue) and $BIPPF_{15}$ (red) at (c) 1548 cm^{-1} and (d) 1597 cm^{-1}. The time range where visible and infrared pulses overlap, <100 fs, is indicated by the shaded area. The error bars show the standard error of the CLS, obtained by a linear fit of the conditional average.[27] The black curve indicates the fit result of the CLS dynamics with a single exponential function. The CLS dynamics of the other observed bands and corresponding fit results is shown in Figures S3–S6.

2DEV Spectroscopy. In order to make definitive assignments and probe further into the dynamics and mechanism of a potential additional unrelaxed PCET pathway in $BIPPF_{15}$, we recorded 2DEV spectra of PF_{15} and $BIPPF_{15}$ (Figure 4a,b). The spectral features of the 2DEV spectra along the excitation axis at 17,000 cm^{-1}, which corresponds to the peak of the optical absorption spectra, were the same as in the transient IR spectra, as expected. The ESA bands at 1597 and 1548 cm^{-1} of $BIPPF_{15}$ become weaker at shorter wavelength excitation, implying that the ultrafast PCET may not depend only on the amount of excess energy. It can also be seen that negative bands at 1546 and 1548 cm^{-1} were observed for PF_{15} and $BIPPF_{15}$, respectively.

The CLS dynamics of these two bands showed significant differences between the two species (Figure 4c). We note that the proton and partial charge have transferred before the temporal range over which we discuss the CLS. In a previous study, we showed that the CLS is directly related to the solvation correlation function for the vibrational degrees of freedom and the time constant of its decay is close to the vibrational dephasing time[26] and more recently provided a detailed derivation for the 2DEV line shape and its evolution.[36] Here, we provide a general, approximate form of the center line slope (CLS) in a 2DEV experiment where we take it to be proportional to the frequency–frequency correlation function[36]

$$\mathrm{CLS} \propto \langle \delta\omega_{\mathrm{elec}}(T)\delta\omega_{\mathrm{vib}}(0)\rangle \tag{1}$$

where $\delta\omega(T)$ is the fluctuating frequency for a given electronic or vibrational transition. We note that, while such a direct proportionality may not hold in every case,[37,38] this approximate form is nonetheless useful to gain intuition for the behavior of the CLS and the governing system dynamics. Particularly, it is straightforward to demonstrate how the CLS in a 2DEV experiment is a cross-correlation between electronic and vibrational dipoles if we simply approximate the fluctuating transition frequency as

$$\delta\omega_{\mathrm{elec}} \propto \Delta\boldsymbol{\mu}_{\mathrm{elec}}\mathbf{E}_{\mathrm{sol}}$$
$$\delta\omega_{\mathrm{vib}} \propto \delta\boldsymbol{\mu}_{\mathrm{vib}}\mathbf{E}_{\mathrm{sol}} \tag{2}$$

where $\Delta\boldsymbol{\mu}_{\mathrm{elec}}$ is the difference in the dipole moment between the ground and excited states of the given transition, $\delta\boldsymbol{\mu}_{\mathrm{vib}}$ is the vibrational Stark tuning rate, and $\boldsymbol{E}_{\mathrm{sol}}$ is the solvent electric field. The resulting form of the CLS can then be written as

$$\mathrm{CLS} \propto \langle \mathbf{E}_{\mathrm{sol}}(T)\cdot[\Delta\boldsymbol{\mu}_{\mathrm{elec}}(T)\delta\boldsymbol{\mu}_{\mathrm{vib}}(0)]\cdot\mathbf{E}_{\mathrm{sol}}(0)\rangle \tag{3}$$

which makes it clear that dynamical changes in the direction and magnitude of the electronic dipoles, in addition to solvent rearrangement, are key drivers of the CLS. For PF_{15}, the CLS of the 1548 cm^{-1} band remained near zero after photoexcitation (Figure 4c, blue), indicating a very similar solvent environment for the mode in both electronic states. On the other hand, for $BIPPF_{15}$, the CLS of the band at 1548 cm^{-1} was positive and essentially constant over 200–500 fs (Figure 4c, red). In this case, the solvent configuration is clearly different after 150 fs and we ascribe the positive CLS to the product of the PCET reaction, which has a large electric dipole moment. This also suggests the presence of an additional, very rapid, unrelaxed pathway for the PCET reaction, with a time scale similar to or less than the current experimental time resolution of ~90 fs. Notably, the CLS of the 1548 cm^{-1} band shows a rise over approximately the initial 200 fs (Figure 4c). However, this band has quite low

https://dx.doi.org/10.1021/jacs.0c10626
J. Am. Chem. Soc. 2021, 143, 3104–3112

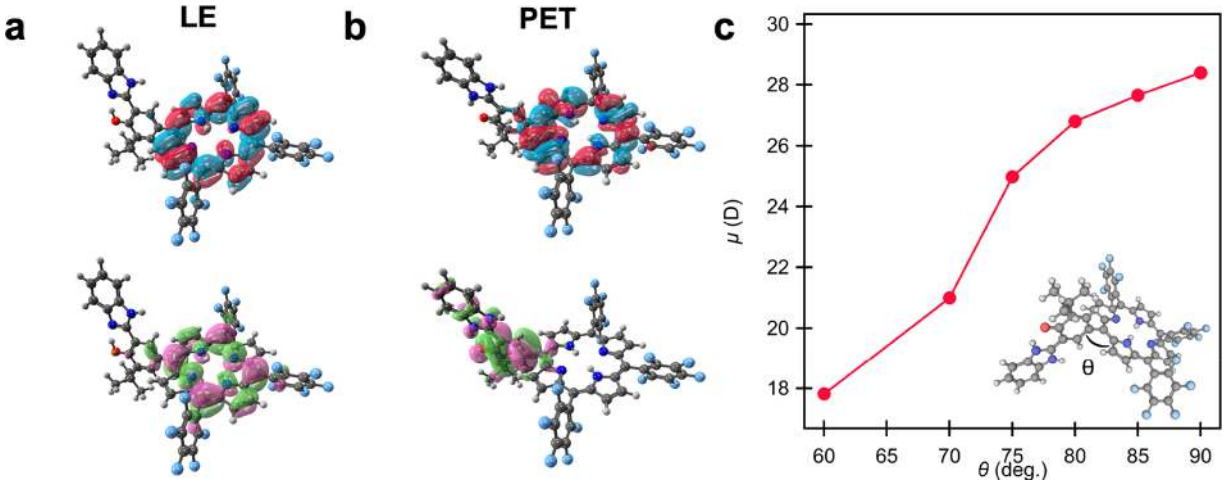

Figure 5. Electronic structure calculation of $BIPPF_{15}$. The dominant NTO pairs for (a) locally excited (LE) and (b) proton and electron transferred (PET) states of $BIPPF_{15}$. For each state, the HONTO is on the bottom and the LUNTO is on the top. (c) Calculated dipole moment of $BIPPF_{15}$ as a function of dihedral angle between BIP and porphyrin moieties. The optimized structure of the PET state of $BIPPF_{15}$ is also shown in the inset.

intensity and thus we turn to a more quantitative discussion of the CLS behavior of the ET band at 1597 cm^{-1} (Figure 4d). The CLS of the 1597 cm^{-1} band is positive and observed to rise to a plateau with a time constant of 120 ± 20 fs. Such a rapid rise was not observed in the transient IR signal of the band at 1597 cm^{-1} (Table S2), which suggests that the underlying physical process is distinct from population dynamics. The CLS is uniquely sensitive to the correlation between electronic and nuclear degrees of freedom and correspondingly contains crucial information on this unrelaxed pathway. To further interpret the rapid changes in the CLS, we turn to electronic structure calculations.

Quantum Chemical Calculations. Quantum chemical calculations were performed within the Born−Oppenheimer approximation, which neglects the quantum-mechanical nature of nuclear motions in utilizing fixed nuclei to parametrize the electronic structure problem. Nevertheless, these calculations provide important insight into the CLS dynamics. The natural transition orbital (NTO)[39] pairs of $BIPPF_{15}$ for the locally excited (LE) and proton and electron transferred (PET) states are shown in Figure 5a,b. For the LE state, both the highest occupied NTO (HONTO) and lowest unoccupied NTO (LUNTO) are localized on the porphyrin moiety, indicating that the permanent electric dipole moments are very similar in both the electronic ground and excited states, resulting in minimal solvent rearrangement upon photoexcitation. As the $BIPPF_{15}$ molecule evolves from the LE state to the PET geometry, the hole (HONTO) localized on the porphyrin moiety moves to the phenol moiety, while the LUNTO essentially remains at the same distribution. This confirms that the PET state is characterized by the transfer of an electron from the BIP to the porphyrin. As the electron density distribution of the PET state is significantly different from that on the ground state potential energy surface and also from that of the LE state, the emergence of a large electric dipole moment in the PET state can be expected to cause a dramatic change in the solvent configuration, which in turn is reflected in the CLS as observed.

In addition, calculations revealed a reaction pathway for the photoinduced PCET, which lays the groundwork for an interpretation of the rise of the CLS. The optimized structures of $BIPPF_{15}$ in the ground state (GS), LE, and PET states are shown in Figure S14. The calculated values of the dihedral angle between BIP and porphyrin subunits are 67.4, 62.6, and 93.1° for the GS, LE (minimum), and PET states. The orthogonal dihedral angle for the PET state is indicative of twisted intramolecular charge transfer (TICT) where the twisting angle plays a significant role in the reaction coordinate, serving to stabilize the CS states.[40] While optimally tuning (OT) the LRC-ωPBEh functional lowers the calculated energy of the PET state by ∼0.42 eV such that it becomes the lowest singlet excited state in the 93.1° geometry, this PET state is predicted to lie above the Franck−Condon LE state (67.4°) by ∼0.27 eV. However, approximating the strong electrostatic interactions between the dipole moment of a TICT state and polar acetonitrile solvent molecules with a polarizable continuum model has been shown to lead to systematically overestimated excitation energies (by as much as ∼0.39 eV) versus experiment even with the OT-LRC-ωPBEh functional.[41] In light of this, our calculation still serves to corroborate our experimental result that this pathway is slightly exergonic (ΔG = −0.10 eV, as determined via electrochemical measurements).

Moreover, to interpret the evolution of the CLS dynamics, the dipole moment of the PET state was calculated as a function of dihedral angle over the range from 60 to 90°, corresponding to the evolution from the minimum of the LE state to the minimum of the PET state (Figure 5c). We note that calculated densities (and therefore, dipole moments) are much less sensitive to the choice of functional than excitation energies and that the LRC-ωPBEh functional employed presently has shown high accuracy in computed dipole moments.[42] It can be seen that the dipole moment increases significantly, from 18 to 28 D, with the increase in the dihedral angle. This is consistent with the following estimate: assuming the center-to-center distance between phenol and porphyrin to be 6.4 Å, the dipole of the system increases by 30.7 D with a complete ET. As the dipole moment of the GS was calculated to be 3.93 D, it can be seen that the degree of the ET in the Franck−Condon region (θ ∼67°) is one-half and it reaches unity as the angle increases.

https://dx.doi.org/10.1021/jacs.0c10626
J. Am. Chem. Soc. 2021, 143, 3104−3112

The above arguments and eq 3 strongly suggest that the 120 fs time scale in the CLS of the 1597 cm^{-1} mode be assigned to the twisting of the dihedral angle with the concomitant charge redistribution leading to a large dipole moment approaching ~30 D (Figure 6). We note that fast

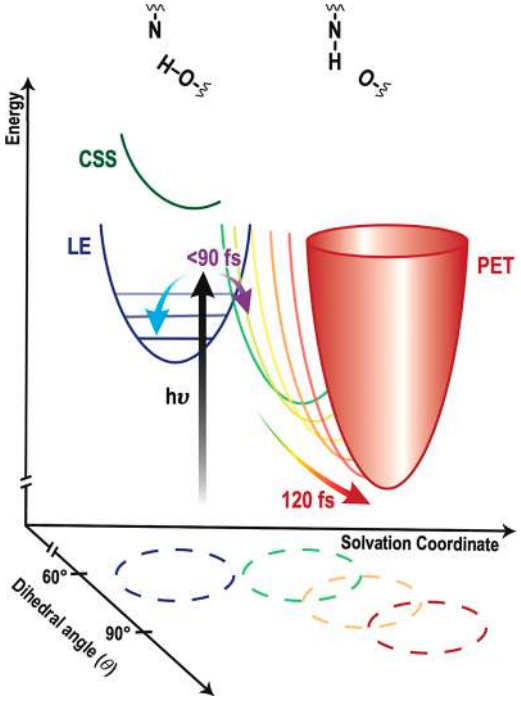

Figure 6. Schematic diagram of ultrafast PCET. Upon photoexcitation, the system is led to the unrelaxed Franck–Condon region and branches into two pathways toward (i) a relaxed locally excited (LE) state (blue arrow), which is followed by a slow PCET pathway (not shown) and can be described as a kinetic phenomenon (Figure 1c where $k_{CS} \ll k_{CR}$), and (ii) an unrelaxed proton and electron transferred (PET) state (purple arrow) within 90 fs. From there, the unrelaxed PET state further rapidly evolves toward the twisted product with concomitant charge localization on a time scale of 120 fs (rainbow arrow). Additionally, it should be noted that the collective solvent response contributes to the reaction coordinate over the course of the ultrafast PCET reaction, as the solvation time scale in acetonitrile[45] is similar to the time scale of twisting. The higher energy charge separated state (CSS) where the proton has not been transferred is not populated.

inertial rotations in TICT systems have also been observed in earlier work by means of visible transient absorption or transient IR spectroscopies.[43,44] In the case of an aniline–triazine donor–acceptor dyad with an alkyne spacer, for example, twisting isomerization dynamics was monitored by the evolution from a vibrational band associated with an alkyne (C≡C—C) to that with an allene (C═C═C) on the time scale of 0.3–2.5 ps, depending on the solvent molecule.[44] However, in 2DEV spectroscopy, the CLS dynamics is free from population dynamics[29] and the current calculation revealed that twisting occurs without significant bond rearrangements. Thus, the rising CLS dynamics reflects the change of the electron density distribution which leads the unrelaxed PET state into the relaxed product, rather than a simple kinetic evolution from LE to PET states.

CONCLUSIONS

Proton-coupled electron transfer in $BIPPF_{1S}$ takes place on two time scales, an ultrafast unrelaxed process from the initial excited levels and a slower relaxed process on the time scale of a few hundred picoseconds. The ultrafast process, though not the dominant pathway, enables us to observe the evolution of the initial, partly charge transferred, state to full charge separation as molecular rearrangement and solvation proceed. The clear rise in the CLS in 120 fs demonstrates that the ET component of the PCET cannot be described as a single kinetic step and the degree of charge transfer begins around 50% and only reaches near unity when a ~90° dihedral angle between BIP and porphyrin components is reached. While such a clearly identifiable nuclear rearrangement is hardly observable in a slower PCET system, it seems highly likely that all PCET systems will require substantial rearrangement to complete the transfers, as they all involve large changes in electronic structure. Thus, the detailed picture of synergistic motions accompanying PCET elucidated by the present combination of experimental and computational techniques provides general insights relevant to PCET and beyond.

ASSOCIATED CONTENT

Supporting Information

The Supporting Information is available free of charge at https://pubs.acs.org/doi/10.1021/jacs.0c10626.

Experimental and theoretical methods, electrochemical data, absorption spectra, fluorescence data, and detailed analysis of transient infrared and electronic–vibrational spectra (PDF)

AUTHOR INFORMATION

Corresponding Author

Graham R. Fleming – *Department of Chemistry, University of California, Berkeley, California 94720, United States; Molecular Biophysics and Integrated Bioimaging Division, Lawrence Berkeley National Laboratory, Berkeley, California 94720, United States; Kavli Energy Nanoscience Institute at Berkeley, Berkeley, California 94720, United States;* orcid.org/0000-0003-0847-1838; Email: grfleming@lbl.gov

Authors

Yusuke Yoneda – *Department of Chemistry, University of California, Berkeley, California 94720, United States; Molecular Biophysics and Integrated Bioimaging Division, Lawrence Berkeley National Laboratory, Berkeley, California 94720, United States; Kavli Energy Nanoscience Institute at Berkeley, Berkeley, California 94720, United States;* orcid.org/0000-0003-4974-6842

S. Jimena Mora – *School of Molecular Sciences, Arizona State University, Tempe, Arizona 85287, United States;* orcid.org/0000-0003-4181-4732

James Shee – *Department of Chemistry, University of California, Berkeley, California 94720, United States;* orcid.org/0000-0001-8333-8151

Brian L. Wadsworth – *School of Molecular Sciences, Arizona State University, Tempe, Arizona 85287, United States; The Biodesign Institute Center for Applied Structural Discovery (CASD), Tempe, Arizona 85287, United States;* orcid.org/0000-0002-0274-9993

https://dx.doi.org/10.1021/jacs.0c10626
J. Am. Chem. Soc. 2021, 143, 3104–3112

Eric A. Arsenault − *Department of Chemistry, University of California, Berkeley, California 94720, United States; Molecular Biophysics and Integrated Bioimaging Division, Lawrence Berkeley National Laboratory, Berkeley, California 94720, United States; Kavli Energy Nanoscience Institute at Berkeley, Berkeley, California 94720, United States*

Diptarka Hait − *Department of Chemistry, University of California, Berkeley, California 94720, United States; Chemical Sciences Division, Lawrence Berkeley National Laboratory, Berkeley, California 94720, United States;* orcid.org/0000-0003-1570-920X

Gerdenis Kodis − *School of Molecular Sciences, Arizona State University, Tempe, Arizona 85287, United States; The Biodesign Institute Center for Applied Structural Discovery (CASD), Tempe, Arizona 85287, United States*

Devens Gust − *School of Molecular Sciences, Arizona State University, Tempe, Arizona 85287, United States;* orcid.org/0000-0003-0550-8498

Gary F. Moore − *School of Molecular Sciences, Arizona State University, Tempe, Arizona 85287, United States; The Biodesign Institute Center for Applied Structural Discovery (CASD), Tempe, Arizona 85287, United States;* orcid.org/0000-0003-3369-9308

Ana L. Moore − *School of Molecular Sciences, Arizona State University, Tempe, Arizona 85287, United States;* orcid.org/0000-0002-6653-9506

Martin Head-Gordon − *Department of Chemistry, University of California, Berkeley, California 94720, United States; Chemical Sciences Division, Lawrence Berkeley National Laboratory, Berkeley, California 94720, United States;* orcid.org/0000-0002-4309-6669

Thomas A. Moore − *School of Molecular Sciences, Arizona State University, Tempe, Arizona 85287, United States;* orcid.org/0000-0002-1577-7117

Complete contact information is available at: https://pubs.acs.org/10.1021/jacs.0c10626

Author Contributions

[▽]Y.Y., S.J.M., J.S., B.L.W.: These authors contributed equally.

Notes

The authors declare no competing financial interest.

■ ACKNOWLEDGMENTS

This research was supported by the Department of Energy, Office of Science, Chemical Sciences, Geosciences and Biosciences Division: G.R.F. (FWP 449A), M.H.-G. (DE-AC02-05CH11231), T.A.M. and A.L.M. (DE-FG02-03ER15393), G.F.M. (DE-SC0021186). This research used resources of the National Energy Research Scientific Computing Center (NERSC), a U.S. Department of Energy Office of Science User Facility operated under Contract No. DE-AC02-05CH11231. Y.Y. appreciates the support of the Japan Society for the Promotion of Science (JSPS) Postdoctoral Fellowship for Research Abroad. E.A.A. acknowledges the support of the Berkeley Fellowship and the National Science Foundation Graduate Research Fellowship (Grant No. DGE 1752814). G.F.M. acknowledges support from the Camille Dreyfus Teacher-Scholar Awards Program. The authors appreciate Dr. Eric Wu for his assistance with the experiments in the preliminary stages of this work.

■ REFERENCES

(1) Huynh, M. H. V.; Meyer, T. J. Proton-Coupled Electron Transfer. *Chem. Rev.* **2007**, *107* (11), 5004−5064.
(2) Meyer, T. J.; Huynh, M. H. V.; Thorp, H. H. The Possible Role of Proton-Coupled Electron Transfer (PCET) in Water Oxidation by Photosystem II. *Angew. Chem., Int. Ed.* **2007**, *46* (28), 5284−5304.
(3) Hammes-Schiffer, S.; Soudackov, A. V. Proton-Coupled Electron Transfer in Solution, Proteins, and Electrochemistry. *J. Phys. Chem. B* **2008**, *112* (45), 14108−14123.
(4) Reece, S. Y.; Nocera, D. G. Proton-Coupled Electron Transfer in Biology: Results from Synergistic Studies in Natural and Model Systems. *Annu. Rev. Biochem.* **2009**, *78* (1), 673−699.
(5) Hammes-Schiffer, S.; Stuchebrukhov, A. A. Theory of Coupled Electron and Proton Transfer Reactions. *Chem. Rev.* **2010**, *110* (12), 6939−6960.
(6) Hammarström, L.; Styring, S. Proton-Coupled Electron Transfer of Tyrosines in Photosystem II and Model Systems for Artificial Photosynthesis: The Role of a Redox-Active Link between Catalyst and Photosensitizer. *Energy Environ. Sci.* **2011**, *4* (7), 2379−2388.
(7) Weinberg, D. R.; Gagliardi, C. J.; Hull, J. F.; Murphy, C. F.; Kent, C. A.; Westlake, B. C.; Paul, A.; Ess, D. H.; McCafferty, D. G.; Meyer, T. J. Proton-Coupled Electron Transfer. *Chem. Rev.* **2012**, *112* (7), 4016−4093.
(8) Mora, S. J.; Odella, E.; Moore, G. F.; Gust, D.; Moore, T. A.; Moore, A. L. Proton-Coupled Electron Transfer in Artificial Photosynthetic Systems. *Acc. Chem. Res.* **2018**, *51* (2), 445−453.
(9) Barry, B. A.; Babcock, G. T. Tyrosine Radicals Are Involved in the Photosynthetic Oxygen-Evolving System. *Proc. Natl. Acad. Sci. U. S. A.* **1987**, *84* (20), 7099−7103.
(10) Barry, B. A. Reaction Dynamics and Proton Coupled Electron Transfer: Studies of Tyrosine-Based Charge Transfer in Natural and Biomimetic Systems. *Biochim. Biophys. Acta, Bioenerg.* **2015**, *1847* (1), 46−54.
(11) Megiatto, J. D.; Antoniuk-Pablant, A.; Sherman, B. D.; Kodis, G.; Gervaldo, M.; Moore, T. A.; Moore, A. L.; Gust, D. Mimicking the Electron Transfer Chain in Photosystem II with a Molecular Triad Thermodynamically Capable of Water Oxidation. *Proc. Natl. Acad. Sci. U. S. A.* **2012**, *109* (39), 15578−15583.
(12) Megiatto, J. D.; Méndez-Hernández, D. D.; Tejeda-Ferrari, M. E.; Teillout, A. L.; Llansola-Portolés, M. J.; Kodis, G.; Poluektov, O. G.; Rajh, T.; Mujica, V.; Groy, T. L.; et al. A Bioinspired Redox Relay That Mimics Radical Interactions of the Tyr-His Pairs of Photosystem II. *Nat. Chem.* **2014**, *6* (5), 423−428.
(13) Ravensbergen, J.; Antoniuk-Pablant, A.; Sherman, B. D.; Kodis, G.; Megiatto, J. D.; Méndez-Hernández, D. D.; Frese, R. N.; van Grondelle, R.; Moore, T. A.; Moore, A. L.; et al. Spectroscopic Analysis of a Biomimetic Model of Tyr Z Function in PSII. *J. Phys. Chem. B* **2015**, *119* (37), 12156−12163.
(14) Huynh, M. T.; Mora, S. J.; Villalba, M.; Tejeda-Ferrari, M. E.; Liddell, P. A.; Cherry, B. R.; Teillout, A.-L.; Machan, C. W.; Kubiak, C. P.; Gust, D.; et al. Concerted One-Electron Two-Proton Transfer Processes in Models Inspired by the Tyr-His Couple of Photosystem II. *ACS Cent. Sci.* **2017**, *3* (5), 372−380.
(15) Odella, E.; Wadsworth, B. L.; Mora, S. J.; Goings, J. J.; Huynh, M. T.; Gust, D.; Moore, T. A.; Moore, G. F.; Hammes-Schiffer, S.; Moore, A. L. Proton-Coupled Electron Transfer Drives Long-Range Proton Translocation in Bioinspired Systems. *J. Am. Chem. Soc.* **2019**, *141* (36), 14057−14061.
(16) Parada, G. A.; Goldsmith, Z. K.; Kolmar, S.; Pettersson Rimgard, B.; Mercado, B. Q.; Hammarström, L.; Hammes-Schiffer, S.; Mayer, J. M. Concerted Proton-Electron Transfer Reactions in the Marcus Inverted Region. *Science* **2019**, *364* (6439), 471−475.
(17) Moore, G. F.; Hambourger, M.; Gervaldo, M.; Poluektov, O. G.; Rajh, T.; Gust, D.; Moore, T. A.; Moore, A. L. A Bioinspired Construct That Mimics the Proton Coupled Electron Transfer between P680 ●+ and the Tyr Z -His190 Pair of Photosystem II. *J. Am. Chem. Soc.* **2008**, *130* (32), 10466−10467.

(18) Wang, D.; Sampaio, R. N.; Troian-Gautier, L.; Marquard, S. L.; Farnum, B. H.; Sherman, B. D.; Sheridan, M. V.; Dares, C. J.; Meyer, G. J.; Meyer, T. J. Molecular Photoelectrode for Water Oxidation Inspired by Photosystem II. *J. Am. Chem. Soc.* **2019**, *141* (19), 7926−7933.
(19) Westlake, B. C.; Brennaman, M. K.; Concepcion, J. J.; Paul, J. J.; Bettis, S. E.; Hampton, S. D.; Miller, S. A.; Lebedeva, N. V.; Forbes, M. D. E.; Moran, A. M.; et al. Concerted Electron-Proton Transfer in the Optical Excitation of Hydrogen-Bonded Dyes. *Proc. Natl. Acad. Sci. U. S. A.* **2011**, *108* (21), 8554−8558.
(20) Eisenhart, T. T.; Dempsey, J. L. Photo-Induced Proton-Coupled Electron Transfer Reactions of Acridine Orange: Comprehensive Spectral and Kinetics Analysis. *J. Am. Chem. Soc.* **2014**, *136* (35), 12221−12224.
(21) Gagliardi, C. J.; Wang, L.; Dongare, P.; Brennaman, M. K.; Papanikolas, J. M.; Meyer, T. J.; Thompson, D. W. Direct Observation of Light-Driven, Concerted Electron-Proton Transfer. *Proc. Natl. Acad. Sci. U. S. A.* **2016**, *113* (40), 11106−11109.
(22) Takeuchi, E.; Muramatsu, M.; Katayama, T.; Yoneda, Y.; Ito, S.; Nagasawa, Y.; Miyasaka, H. Sub-100 Fs Charge Separation and Subsequent Diffusive Solvation Observed for Asymmetric Bianthryl Derivative in Ionic Liquid. *J. Phys. Chem. C* **2016**, *120* (27), 14502−14512.
(23) Yoneda, Y.; Sotome, H.; Mathew, R.; Lakshmanna, Y. A.; Miyasaka, H. Non-Condon Effect on Ultrafast Excited-State Intramolecular Proton Transfer. *J. Phys. Chem. A* **2020**, *124* (2), 265−271.
(24) Hazra, A.; Soudackov, A. V.; Hammes-Schiffer, S. Isotope Effects on the Nonequilibrium Dynamics of Ultrafast Photoinduced Proton-Coupled Electron Transfer Reactions in Solution. *J. Phys. Chem. Lett.* **2011**, *2* (1), 36−40.
(25) Oliver, T. A. A.; Lewis, N. H. C.; Fleming, G. R. Correlating the Motion of Electrons and Nuclei with Two-Dimensional Electronic-Vibrational Spectroscopy. *Proc. Natl. Acad. Sci. U. S. A.* **2014**, *111* (28), 10061−10066.
(26) Lewis, N. H. C.; Dong, H.; Oliver, T. A. A.; Fleming, G. R. Measuring Correlated Electronic and Vibrational Spectral Dynamics Using Line Shapes in Two-Dimensional Electronic-Vibrational Spectroscopy. *J. Chem. Phys.* **2015**, *142* (17), 174202.
(27) Wu, E. C.; Ge, Q.; Arsenault, E. A.; Lewis, N. H. C.; Gruenke, N. L.; Head-Gordon, M. J.; Fleming, G. R. Two-Dimensional Electronic-Vibrational Spectroscopic Study of Conical Intersection Dynamics: An Experimental and Electronic Structure Study. *Phys. Chem. Chem. Phys.* **2019**, *21* (26), 14153−14163.
(28) Gaynor, J. D.; Sandwisch, J.; Khalil, M. Vibronic Coherence Evolution in Multidimensional Ultrafast Photochemical Processes. *Nat. Commun.* **2019**, *10* (1), 5621.
(29) Arsenault, E. A.; Yoneda, Y.; Fleming, G. R.; Niyogi, K. K.; Iwai, M.; Niyogi, K. K.; Fleming, G. R. Vibronic Mixing Enables Ultrafast Energy Flow in Light-Harvesting Complex II. *Nat. Commun.* **2020**, *11* (1), 1460.
(30) Mora, S. J.; Heredia, D. A.; Odella, E.; Vrudhula, U.; Gust, D.; Moore, T. A.; Moore, A. L. Design and Synthesis of Benzimidazole Phenol-Porphyrin Dyads for the Study of Bioinspired Photoinduced Proton-Coupled Electron Transfer. *J. Porphyrins Phthalocyanines* **2019**, *23* (11−12), 1336−1345.
(31) Iikura, H.; Tsuneda, T.; Yanai, T.; Hirao, K. A Long-Range Correction Scheme for Generalized-Gradient-Approximation Exchange Functionals. *J. Chem. Phys.* **2001**, *115* (8), 3540−3544.
(32) Tawada, Y.; Tsuneda, T.; Yanagisawa, S.; Yanai, T.; Hirao, K. A Long-Range-Corrected Time-Dependent Density Functional Theory. *J. Chem. Phys.* **2004**, *120* (18), 8425−8433.
(33) Stein, T.; Eisenberg, H.; Kronik, L.; Baer, R. Fundamental Gaps in Finite Systems from Eigenvalues of a Generalized Kohn-Sham Method. *Phys. Rev. Lett.* **2010**, *105* (26), 266802.
(34) Körzdörfer, T.; Brédas, J.-L. Organic Electronic Materials: Recent Advances in the DFT Description of the Ground and Excited States Using Tuned Range-Separated Hybrid Functionals. *Acc. Chem. Res.* **2014**, *47* (11), 3284−3291.
(35) Stein, T.; Kronik, L.; Baer, R. Reliable Prediction of Charge Transfer Excitations in Molecular Complexesusing Time-Dependent Density Functional Theory. *J. Am. Chem. Soc.* **2009**, *131* (8), 2818−2820.
(36) Cho, M.; Fleming, G. R. Two-Dimensional Electronic−Vibrational Spectroscopy Reveals Cross-Correlation between Solvation Dynamics and Vibrational Spectral Diffusion. *J. Phys. Chem. B* **2020**, *124* (49), 11222−11235.
(37) Kwak, K.; Park, S.; Finkelstein, I. J.; Fayer, M. D. Frequency-Frequency Correlation Functions and Apodization in Two-Dimensional Infrared Vibrational Echo Spectroscopy: A New Approach. *J. Chem. Phys.* **2007**, *127* (12), 124503.
(38) Kwak, K.; Rosenfeld, D. E.; Fayer, M. D. Taking Apart the Two-Dimensional Infrared Vibrational Echo Spectra: More Information and Elimination of Distortions. *J. Chem. Phys.* **2008**, *128* (20), 204505.
(39) Martin, R. L. Natural Transition Orbitals. *J. Chem. Phys.* **2003**, *118* (11), 4775−4777.
(40) Grabowski, Z. R.; Rotkiewicz, K.; Rettig, W. Structural Changes Accompanying Intramolecular Electron Transfer: Focus on Twisted Intramolecular Charge-Transfer States and Structures. *Chem. Rev.* **2003**, *103* (10), 3899−4031.
(41) Shee, J.; Head-Gordon, M. Predicting Excitation Energies of Twisted Intramolecular Charge-Transfer States with the Time-Dependent Density Functional Theory: Comparison with Experimental Measurements in the Gas Phase and Solvents Ranging from Hexanes to Acetonitrile. *J. Chem. Theory Comput.* **2020**, *16* (10), 6244−6255.
(42) Hait, D.; Head-Gordon, M. How Accurate Is Density Functional Theory at Predicting Dipole Moments? An Assessment Using a New Database of 200 Benchmark Values. *J. Chem. Theory Comput.* **2018**, *14* (4), 1969−1981.
(43) Martin, M. M.; Plaza, P.; Changenet-Barret, P.; Siemiarczuk, A. UV-Vis Subpicosecond Spectroscopy of 4-(9-Anthryl)-N,N′-Dimethylaniline in Polar and Nonpolar Solvents: A Two-Dimensional View of the Photodynamics. *J. Phys. Chem. A* **2002**, *106* (10), 2351−2358.
(44) Dereka, B.; Svechkarev, D.; Rosspeintner, A.; Tromayer, M.; Liska, R.; Mohs, A. M.; Vauthey, E. Direct Observation of a Photochemical Alkyne-Allene Reaction and of a Twisted and Rehybridized Intramolecular Charge-Transfer State in a Donor-Acceptor Dyad. *J. Am. Chem. Soc.* **2017**, *139* (46), 16885−16893.
(45) Rosenthal, S. J.; Xie, X.; Du, M.; Fleming, G. R. Femtosecond Solvation Dynamics in Acetonitrile: Observation of the Inertial Contribution to the Solvent Response. *J. Chem. Phys.* **1991**, *95* (6), 4715−4718.

https://dx.doi.org/10.1021/jacs.0c10626
J. Am. Chem. Soc. 2021, 143, 3104−3112